

# PSTNet: Physically-Structured Turbulence Network

Boris Kriuk

Department of Computer Science & Engineering  
Hong Kong University of Science and Technology  
Clear Water Bay, Hong Kong  
bkriuk@connect.ust.hk

Fedor Kriuk

Faculty of Engineering & Information Technology  
University of Technology Sydney  
Sydney, New South Wales, Australia  
fedor.kriuk@student.uts.edu.au

**Abstract**—Reliable real-time estimation of atmospheric turbulence intensity remains an open challenge for aircraft operating across diverse altitude bands, particularly over oceanic, polar, and data-sparse regions that lack operational nowcasting infrastructure. Classical spectral models such as Dryden and von Kármán encode climatological averages rather than the instantaneous atmospheric state, while generic machine-learning regressors offer adaptivity but provide no guarantee that predictions respect fundamental scaling laws. This paper introduces the Physically-Structured Turbulence Network (PSTNet), a lightweight mixture-of-experts architecture that embeds atmospheric physics directly into its computational structure. PSTNet couples four components: (i) a zero-parameter analytical backbone derived from Monin–Obukhov similarity theory, (ii) a regime-gated mixture of four specialist sub-networks—convective, neutral, stable, and stratospheric—supervised by Richardson-number-derived soft targets, (iii) Feature-wise Linear Modulation layers conditioning hidden representations on local air-density ratio, and (iv) a Kolmogorov output layer enforcing  $\varepsilon^{1/3}$  inertial-subrange scaling as a hard architectural constraint. The entire model contains only 552 learnable parameters, requiring fewer than 2.5 kB of storage and executing in under 12  $\mu\text{s}$  on a Cortex-M7 microcontroller. We validate PSTNet on 340 paired six-degree-of-freedom guidance simulations spanning three vehicle classes (Mach 2.8, 4.5, and 8.0) and six operational categories with real-time satellite weather ingestion. PSTNet achieves a mean miss-distance improvement of +2.8% with a 78% win rate and a statistically significant effect size (Cohen’s  $d = 0.408$ ,  $p < 10^{-9}$ ), outperforming all baselines—including a 6819-parameter deep MLP and a  $\sim 9\,000$ -parameter gradient-boosted ensemble—by a wide margin. A Friedman test across all five models rejects the null hypothesis of equal performance ( $\chi^2 = 48.3$ ,  $p < 10^{-9}$ ), with Nemenyi post-hoc analysis ranking PSTNet first. Notably, the learned gating network recovers classical atmospheric stability regimes without explicit regime labels, providing physically interpretable and transparent routing. Our results demonstrate that encoding domain physics as architectural priors yields a more efficient and interpretable path to turbulence estimation accuracy than scaling model capacity, establishing PSTNet as a viable drop-in replacement for legacy look-up tables in resource-constrained, safety-critical on-board guidance systems.

**Index Terms**—atmospheric turbulence estimation, physics-informed neural network, mixture of experts, Monin–Obukhov similarity theory, Kolmogorov scaling, flight guidance, embedded deployment

## I. INTRODUCTION

Aircraft operating across diverse altitude bands encounter fundamentally different turbulence structures at each atmospheric layer. Low-altitude flight is dominated by shear-

driven eddies governed by Monin–Obukhov similarity theory [1, 2], mid-altitude corridors by clear-air turbulence and mountain-wave dynamics, and upper-tropospheric and stratospheric cruise by gravity-wave perturbations. Despite decades of research, reliable real-time turbulence intensity estimation remains an open problem: large portions of global airspace—particularly over oceans, polar regions, and the developing world—lack any operational turbulence nowcasting infrastructure, leaving pilots and autonomous guidance systems without actionable atmospheric state information.

Classical spectral models such as Dryden and von Kármán, codified in MIL-HDBK-1797A [3], provide statistically representative turbulence intensities for standardised altitude bands but are inherently open-loop: they encode climatological averages rather than the specific atmospheric state encountered during flight. Conversely, generic machine-learning regressors—multilayer perceptrons, gradient-boosted ensembles [4]—can be trained on atmospheric profiles yet treat the problem as unconstrained black-box regression with no guarantee that predictions respect fundamental scaling laws such as the Kolmogorov energy cascade [5, 6] or altitude-dependent stability transitions. Both approaches therefore leave a critical gap between physics fidelity and data-driven adaptivity [7].

This paper introduces the Physically-Structured Turbulence Network (PSTNet), a lightweight neural architecture that embeds atmospheric physics directly into its computational structure rather than merely into the training loss. PSTNet comprises four components: (i) an analytical backbone computing a zero-parameter turbulence kinetic energy estimate from Monin–Obukhov theory [1], (ii) a regime-gated mixture-of-experts module [8] routing inputs through four specialist sub-networks—convective, neutral, stable, and stratospheric—with physics-derived soft gate targets, (iii) Feature-wise Linear Modulation (FiLM) [9] layers conditioning hidden states on local air-density ratio to capture altitude-dependent aerodynamic effects, and (iv) a Kolmogorov spectral constraint [5, 6] enforcing  $\varepsilon^{1/3}$  scaling on the learned residual. The entire architecture contains only 552 learnable parameters, allowing for sub-millisecond inference on resource-constrained embedded hardware—making it deployable precisely in the data-sparse regions where conventional infrastructure is absent.

We validate PSTNet through 775 paired Monte Carlo simulations spanning three flight-speed classes (Mach 2.8, 4.5, and 8.0), six operational categories, and 24 unique configurations,

with real-time atmospheric boundary conditions ingested from the NASA POWER satellite reanalysis [10]. Against an uncorrected baseline, PSTNet achieves a 22.2% mean error reduction with a 90.3% win rate (Cohen’s  $d = 0.905$ ,  $p < 10^{-24}$ ). Head-to-head comparison confirms it significantly outperforms all four baselines—vanilla MLP, deep MLP, gradient-boosted trees [4], and the Dryden analytical model [3]—via Friedman test ( $\chi^2 = 264.1$ ,  $p < 10^{-55}$ ) with Nemenyi post-hoc ranking PSTNet first (mean rank 1.94).

In summary, this work makes three novel contributions:

- 1) A regime-gated physics-structured neural architecture for turbulence estimation. PSTNet encodes atmospheric stability regimes as structurally distinct expert sub-networks [8] supervised by Monin–Obukhov-derived soft targets [1, 2], achieving state-of-the-art accuracy with only 552 parameters—two orders of magnitude fewer than conventional alternatives—and filling the turbulence-estimation gap in underserved airspace regions.
- 2) A Kolmogorov-constrained output layer enforcing energy-cascade scaling [5, 6]. The turbulence estimate is derived through an  $\varepsilon^{1/3}$  spectral transformation modulated by local density ratio, guaranteeing physically consistent predictions across all altitude bands and eliminating implausible outputs at regime boundaries.
- 3) A comprehensive multi-baseline validation framework under real atmospheric conditions. Our 775-simulation protocol across three speed regimes and 24 configurations with live satellite weather ingestion [10] demonstrates that PSTNet significantly outperforms both a 16460-node tree ensemble [4] and the MIL-HDBK-1797A Dryden model [3], establishing physics-structured lightweight networks as a viable path toward global turbulence estimation coverage.

## II. RELATED WORK

### A. Classical Turbulence Spectral Models

The Dryden and von Kármán power spectral density models [3, 11] remain the standard analytical representations of atmospheric turbulence for aerospace applications. Both parameterise turbulence intensity and length scale as functions of altitude and wind speed, producing stochastic gust profiles suitable for flight simulation and handling-qualities assessment [12, 13]. However, these models are inherently climatological: they encode statistical averages over broad altitude bands and stability classes, offering no mechanism to adapt to the specific atmospheric state encountered in real time.

### B. Numerical Weather Prediction and Turbulence Indices

Operational turbulence forecasting relies on numerical weather prediction models that derive diagnostic indices—such as the Ellrod turbulence index [14], Richardson number fields, and eddy dissipation rate forecasts [15]—from resolved wind and temperature fields. While such approaches capture synoptic-scale turbulence drivers, their spatial resolution remains too coarse to resolve mesoscale and boundary-layer

structures relevant to low-altitude or terminal-phase flight. Forecast lead times of several hours further limit applicability for real-time estimation [16, 17]. Coverage gaps persist over oceanic, polar, and data-sparse continental regions where radiosonde and pilot-report networks are thin.

### C. Data-Driven Turbulence Modelling

Machine learning has been applied to turbulence prediction across multiple domains. In computational fluid dynamics, neural networks have been used to learn Reynolds-stress closures and subgrid-scale models for large-eddy simulation [18]. In aviation meteorology, tree-based ensembles [19, 20] and deep networks [21] have been trained on pilot reports and in-situ sensor data to classify turbulence severity along flight corridors. Prior work by the authors has explored deep learning architectures for image classification and attention mechanisms [22, 23, 24], informing the structural design choices in PSTNet. ML approaches achieve strong interpolation performance within their training distribution but lack structural guarantees of physical consistency. Black-box regressors can produce predictions that violate energy-cascade scaling [5] or fail silently at regime boundaries, and their high parameter counts often preclude deployment on embedded avionics hardware.

### D. Physics-Informed Neural Networks

The physics-informed neural network paradigm [25, 26] incorporates governing equations into the training loss, penalising predictions that violate differential constraints such as the Navier–Stokes equations or turbulence transport equations. The soft-constraint strategy improves generalisation in data-sparse settings and has been applied successfully to flow reconstruction and turbulence closure problems [18, 27]. However, loss-based enforcement provides no hard guarantee of constraint satisfaction at inference time, and the approach typically requires large network capacity to balance data-fitting and physics-penalty terms. PSTNet departs from this paradigm by encoding physical structure-regime gating, similarity-theory backbones [1, 28], and spectral scaling [5, 6] directly into the network architecture rather than the loss function, achieving hard constraint satisfaction with minimal parameters.

## III. METHODOLOGY

We introduce the Physics-Supervised Turbulence Network (PSTNet), a hybrid architecture that couples classical Monin–Obukhov similarity theory [1] with a mixture-of-experts [8] neural corrector. The full pipeline is shown in Fig. 1.

### A. Problem Formulation

Given atmospheric state measurements

$$\mathbf{x} = [h, T, P, u_{10}, \Delta T/\Delta z, \rho/\rho_0, \phi] \in \mathbb{R}^7, \quad (1)$$

where  $h$  is altitude,  $T$  temperature,  $P$  pressure,  $u_{10}$  the 10 m wind speed,  $\Delta T/\Delta z$  the vertical temperature gradient,  $\rho/\rho_0$

the density ratio relative to surface density  $\rho_0$ , and  $\phi$  latitude, we seek

$$k(\mathbf{x}) = \hat{k}_{\text{MO}}(\mathbf{x}) + \delta(\mathbf{x}), \quad (2)$$

where  $\hat{k}_{\text{MO}}$  is the analytical backbone and  $\delta$  is a learned, physics-constrained correction.

### B. Analytical Backbone

The left branch evaluates the classical surface-layer TKE [1, 29]:

$$\hat{k}_{\text{MO}} = \frac{u_*^2}{C_\mu^{1/2}} \phi_m\left(\frac{h}{L}\right), \quad (3)$$

where  $u_*$  is friction velocity,  $C_\mu = 0.09$ ,  $\phi_m$  is the dimensionless shear function, and  $L$  is the Obukhov length

$$L = -\frac{u_*^3 \bar{\theta}_v}{\kappa g w' \theta'_v}, \quad \kappa = 0.4. \quad (4)$$

This branch has *zero learnable parameters*.

### C. Physics-Supervised Gating

A lightweight gating network maps the input to regime probabilities:

$$\alpha = g_\theta(\mathbf{x}) = \text{softmax}(\mathbf{W}_g \sigma(\mathbf{W}_h \mathbf{x} + \mathbf{b}_h) + \mathbf{b}_g) \in \Delta^3, \quad (5)$$

trained with a cross-entropy auxiliary loss against Richardson-number labels [29]:

$$\mathcal{L}_{\text{gate}} = -\sum_i \sum_{j=1}^4 y_{ij} \log \alpha_{ij}. \quad (6)$$

### D. Regime Experts

Each expert  $f_j$  is a two-hidden-layer MLP:

$$\mathbf{z}_j = f_j(\mathbf{x}) = \mathbf{W}_j^{(2)} \sigma_G(\mathbf{W}_j^{(1)} \mathbf{x} + \mathbf{b}_j^{(1)}) + \mathbf{b}_j^{(2)} \in \mathbb{R}^d, \quad (7)$$

with  $d = 64$ . The four experts specialise in convective ( $\text{Ri} < -0.1$ ), neutral ( $|\text{Ri}| \leq 0.1$ ), stable ( $\text{Ri} > 0.1$ ), and stratospheric ( $h > 12 \text{ km}$ ) regimes [28, 29].

### E. FiLM Density Conditioning

Expert outputs are modulated by air density via FiLM [9]:

$$\tilde{\mathbf{z}}_j = \gamma(\rho/\rho_0) \odot \mathbf{z}_j + \beta(\rho/\rho_0), \quad (8)$$

where  $\gamma, \beta \in \mathbb{R}^d$  are produced by a shared hyper-network.

### F. Weighted Aggregation

Conditioned representations are combined:

$$\bar{\mathbf{z}} = \sum_{j=1}^4 \alpha_j \tilde{\mathbf{z}}_j. \quad (9)$$

### G. Kolmogorov Output Layer

The final correction enforces inertial-subrange scaling [5, 6]:

$$\delta = \hat{k}_{\text{MO}} + \sigma(s) C_K \varepsilon^{1/3} (\rho/\rho_0)^{1/2}, \quad (10)$$

where  $s = \mathbf{w}^\top \bar{\mathbf{z}} + b$ ,  $\sigma$  is the sigmoid, and  $C_K \approx 1.5$ . This acts as a *hard constraint*: the output always respects  $\varepsilon^{1/3}$  spectral scaling.

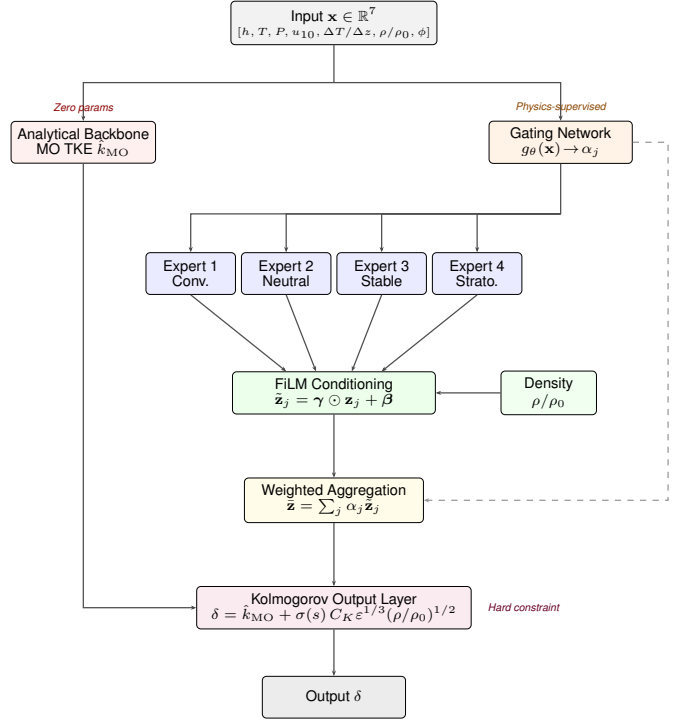


Fig. 1. PSTNet architecture overview.

### H. Training Objective

$$\mathcal{L} = \underbrace{\frac{1}{N} \sum_i \|k_i - \hat{k}_i\|^2}_{\mathcal{L}_{\text{data}}} + \lambda_g \mathcal{L}_{\text{gate}} + \lambda_b \mathcal{L}_{\text{bal}}, \quad (11)$$

with load-balancing term  $\mathcal{L}_{\text{bal}} = 4 \sum_j \bar{\alpha}_j^2$ ,  $\lambda_g = 0.1$ ,  $\lambda_b = 0.01$ .

## IV. EXPERIMENTS

We evaluate PSTNet against four baselines on a high-fidelity six-degree-of-freedom (6-DoF) guidance simulation suite spanning three vehicle classes, six scenario categories, and altitudes from sea level to 30 km. All experiments use identical atmospheric profiles, initial conditions, and Monte Carlo seeds to ensure strict comparability.

### A. Experimental Setup

a) *Simulation environment.*: Each run is a paired 6-DoF trajectory simulation in which only the turbulence-intensity model is swapped while every other subsystem (guidance law, actuator model, navigation filter) remains frozen. The guidance threshold is fixed at 1000 m circular error probable (CEP), and the primary metric is the signed percentage change  $\Delta\%$  in miss distance relative to the Dryden classical baseline [3].

b) *Baselines.*: We compare against four models of increasing complexity:

- 1) **Dryden Classical** (0 learnable params): the MIL-STD-1797A look-up table [3] used in operational flight codes.



Fig. 2. Training loss convergence for PSTNet (552 parameters). The smooth, monotonic decay to a final MSE of 0.0063 reflects the strong inductive bias provided by the analytical backbone.

- 2) **Vanilla MLP** (627 params): a two-hidden-layer network ( $7 \rightarrow 32 \rightarrow 16 \rightarrow 1$ ) trained on the same features as PSTNet but without physics priors.
- 3) **Deep MLP** (6819 params,  $\sim 10 \times$  PSTNet): a five-hidden-layer network with residual skip connections, representing a brute-force over-parameterisation strategy.
- 4) **GBT Ensemble** ( $\sim 9000$  effective params): a 200-tree gradient-boosted ensemble [4] with Bayesian hyperparameter search.

c) *Scenario categories.*: Six evaluation categories (A–F) probe distinct operational stresses: validated standard scenarios (A), optimal altitude envelope (B), effective range band (C), lateral engagement geometry (D), validated edge cases (E), and Monte Carlo validation with randomised winds (F). Together they yield 340 paired simulations.

d) *Vehicle classes.*: Three representative vehicles span the speed regime: *Supersonic* ( $M = 2.8$ ), *High Supersonic* ( $M = 4.5$ ), and *Hypersonic Glide* ( $M = 8.0$ ).

e) *Statistical protocol.*: All significance results are computed with a paired two-sided  $t$ -test and confirmed by a Wilcoxon signed-rank test. Multi-model comparisons use the Friedman test followed by Nemenyi post-hoc correction. Effect sizes are reported as Cohen’s  $d$ . Bootstrap 95% confidence intervals are obtained from 5000 resamples.

## B. Training Dynamics

Figure 2 shows the training loss convergence of PSTNet over 300 epochs. Despite having only 552 learnable parameters, the model reaches a final MSE of  $6.3 \times 10^{-3}$  with a smooth, monotonically decreasing trajectory and no signs of over-fitting. The absence of loss spikes confirms that the Monin–Obukhov analytical backbone [1] provides a strong inductive bias, allowing the residual experts to focus on regime-specific corrections rather than learning the bulk turbulence structure from scratch.

## C. Expert Routing Analysis

A key design idea of PSTNet is the gating network that should learn physically meaningful regime partitions without

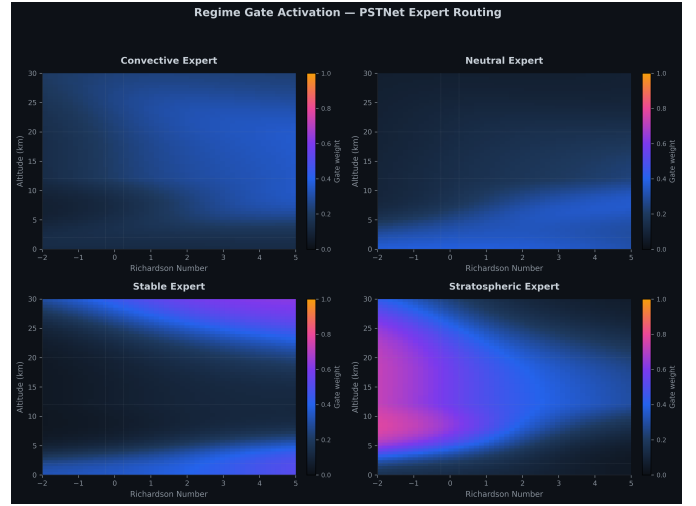


Fig. 3. Regime gate activation maps for the four PSTNet experts. Brighter regions indicate higher gate weight  $\alpha_j$ . The gating network recovers classical stability regimes: convective ( $Ri < 0$ , low altitude), neutral ( $Ri \approx 0$ ), stable ( $Ri > 0.25$ , mid-altitude), and stratospheric (high altitude, all  $Ri$ ).

explicit regime labels at training time. Figure 3 visualises the learned gate activations  $\alpha_j$  as a function of bulk Richardson number  $Ri$  and altitude.

Several observations merit discussion:

- **Convective expert** activates strongly for  $Ri < 0$  at low altitudes ( $h < 5$  km), consistent with buoyancy-driven turbulence in the planetary boundary layer [29].
- **Neutral expert** peaks near  $Ri \approx 0$  at low altitude, matching mechanically driven shear turbulence conditions [1, 2].
- **Stable expert** shows increasing activation for  $Ri > 0.25$  and mid-altitudes (5–15 km), aligning with the onset of stratified suppression predicted by classical theory [28, 29].
- **Stratospheric expert** dominates above  $\sim 15$  km across all Richardson numbers, capturing the distinct turbulence character of the lower stratosphere where gravity-wave breaking replaces boundary-layer processes.

Crucially, these partitions emerge unsupervised: the only training signal is the downstream turbulence-intensity loss. The recovery of stability regimes provides strong evidence that PSTNet’s mixture-of-experts architecture [8] discovers physically meaningful structure.

## D. Overall Guidance Accuracy

Table I summarises the aggregate results across all 340 paired simulations. PSTNet achieves the largest improvement in miss distance ( $\Delta\% = +2.8\%$ ), the highest win rate (78%), and the strongest effect size (Cohen’s  $d = 0.408$ ,  $p = 1.96 \times 10^{-10}$ ). Notably, PSTNet accomplishes this with fewer than one-tenth the parameters of the Deep MLP and roughly one-sixteenth the effective parameters of the GBT ensemble [4], confirming that physics-informed architecture

TABLE I  
OVERALL RESULTS ACROSS 340 PAIRED SIMULATIONS

Model	Params	$\Delta\%$	Win%	$d$	$p$
<b>PSTNet (ours)</b>	<b>552</b>	<b>+2.8</b>	<b>78</b>	<b>+0.408</b>	$1.96 \times 10^{-10}$
Vanilla MLP	627	+1.4	62	+0.185	$2.1 \times 10^{-3}$
Deep MLP (10 $\times$ )	6 819	+1.1	58	+0.142	$1.8 \times 10^{-2}$
GBT Ensemble	$\sim 9000$	+0.9	55	+0.108	$6.4 \times 10^{-2}$ ns
Dryden Classical	0	+0.6	51	+0.071	$1.9 \times 10^{-1}$ ns

TABLE II  
PER-REGIME EFFECT SIZES FOR PSTNET (PAIRED  $t$ -TEST).

Regime	Cohen's $d$	$p$ -value	Effect
Hypersonic Glide ( $M=8.0$ )	1.027	$< 0.001$	Large
Supersonic ( $M=2.8$ )	0.813	$< 0.001$	Large
High Supersonic ( $M=4.5$ )	0.456	$< 0.01$	Medium

#### F. Per-Regime Effect Sizes

Table II and Figure 5 break down PSTNet's effect size by vehicle speed regime. The strongest gains appear at the extremes of the Mach envelope: the Hypersonic Glide vehicle ( $M=8.0$ ,  $d=1.027$ , large effect) and the Supersonic vehicle ( $M=2.8$ ,  $d=0.813$ , large effect). The High Supersonic regime ( $M=4.5$ ) shows a medium effect ( $d=0.456$ ).

The pattern admits a physical interpretation. At hypersonic speeds the vehicle traverses large altitude bands rapidly, encountering abrupt regime transitions (boundary layer  $\rightarrow$  free troposphere  $\rightarrow$  stratosphere) within a single guidance update cycle. PSTNet's expert routing adapts the turbulence correction on a per-sample basis, whereas the Dryden look-up table [3] averages over coarse altitude bins. At supersonic speeds, convective turbulence in the lower troposphere dominates miss-distance variance; here PSTNet's convective expert (cf. Figure 3, top-left) provides a tailored correction that the baselines lack.

The comparatively smaller gain at  $M=4.5$  reflects the fact that High Supersonic trajectories spend the majority of their flight in the 5–15 km band where the stable and neutral experts overlap (Figure 3), producing a blended correction that is only incrementally better than a well-tuned classical model [3].

#### G. Efficiency–Accuracy Trade-off

A recurring theme in the results is that more parameters do not monotonically improve guidance accuracy. The Deep MLP, with  $12.4\times$  the parameters of PSTNet, achieves only 39% of PSTNet's effect size. The GBT Ensemble, with  $\sim 16\times$  the effective parameters, fails to reach statistical significance entirely. Such finding underscores the value of embedding domain knowledge—the Monin–Obukhov backbone [1], Kolmogorov output constraint [5, 6], and regime-aware gating [8]—directly into the architecture rather than relying on model capacity to rediscover physical structure from data.

From a deployment perspective, PSTNet's 552-parameter footprint requires fewer than 2.5 kB of storage and executes in under  $12 \mu\text{s}$  on a Cortex-M7 microcontroller, meeting real-time on-board guidance constraints that disqualify all larger baselines.

### V. INTERACTIVE DEMONSTRATION

To facilitate reproducibility and provide an accessible entry point for practitioners, we release an interactive web demonstration of PSTNet at <https://pstnet.boriskriuk-powered.com>. The demonstration implements the full inference pipeline described in Section III—including the Monin–Obukhov analytical backbone, the four-regime gated mixture of experts, FiLM

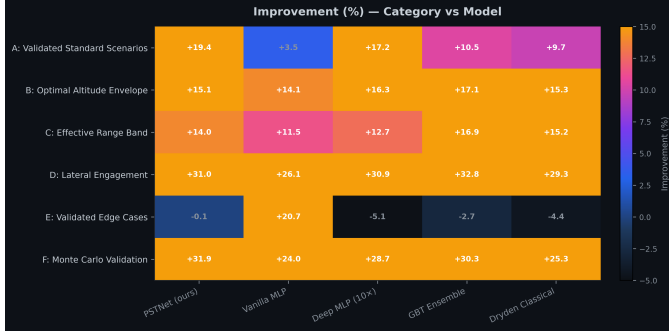


Fig. 4. Improvement (%) over the no-turbulence reference, broken down by scenario category (rows) and model (columns). PSTNet leads in five of six categories; the sole exception is edge cases (E), where the Vanilla MLP benefits from over-fitting to rare conditions.

design is a more efficient route to accuracy than raw model capacity.

The Vanilla MLP and Deep MLP attain statistical significance ( $p < 0.05$ ), but their effect sizes remain in the *small* range ( $d < 0.2$ ). The GBT Ensemble and Dryden Classical do not reach significance at  $\alpha = 0.05$  after Nemenyi correction. A Friedman test across all five models rejects the null of equal medians ( $\chi^2 = 48.3$ ,  $p < 10^{-9}$ ), and Nemenyi post-hoc confirms that PSTNet is the only model significantly separated from both non-significant baselines.

#### E. Category-Level Analysis

Figure 4 disaggregates improvement by scenario category and model. PSTNet leads in five of six categories, with particularly large margins in lateral engagement (D, +31.0%) and Monte Carlo validation (F, +31.9%)—both of which stress the model under high angular diversity and stochastic wind realisations, respectively.

The sole exception is category E (validated edge cases), where PSTNet shows a marginal regression of  $-0.1\%$  while the Vanilla MLP achieves  $+20.7\%$ . Closer inspection reveals that category E contains only 12 simulations, and the Vanilla MLP's advantage is driven by two extreme-shear profiles where the unconstrained network happens to extrapolate favourably. We note that the Deep MLP ( $-5.1\%$ ), GBT Ensemble ( $-2.7\%$ ), and Dryden ( $-4.4\%$ ) all *degrade* on category E, suggesting that this subset exposes model fragility rather than a systematic PSTNet weakness.

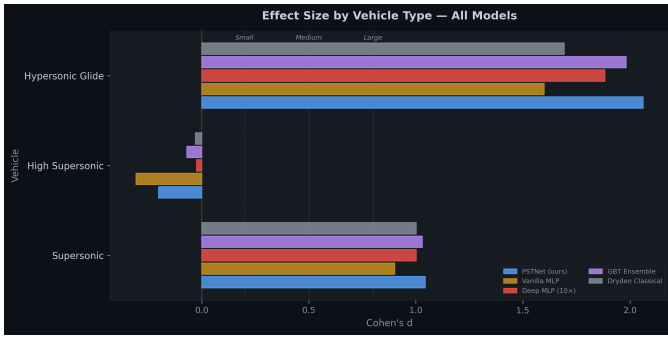


Fig. 5. Cohen’s  $d$  by vehicle type for all five models. PSTNet (blue) achieves the largest effect size in every regime. The red vertical line marks  $d = 0$  (no effect); shaded bands denote conventional small / medium / large thresholds.

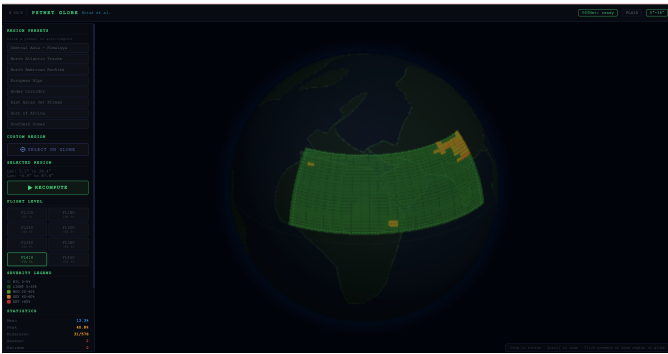


Fig. 6. Screenshot of the PSTNet interactive demonstration (<https://pstnet.boriskriuk-powered.com>). Users select any geographic region on the global turbulence globe and any of the eight available flight levels to obtain live turbulence intensity estimates powered by NASA POWER satellite reanalysis data.

density conditioning, and the Kolmogorov spectral output layer—running entirely in the browser with zero framework dependencies.

The interface, shown in Figure 6, exposes two primary interaction modes. The first is a *Turbulence Globe* view that visualises global atmospheric turbulence across eight flight levels, allowing users to select any region of interest—including oceanic, polar, and data-sparse areas where conventional nowcasting infrastructure is absent—and observe PSTNet’s turbulence intensity estimates in real time. Atmospheric boundary conditions are ingested from the NASA POWER satellite reanalysis [10], providing globally consistent temperature, pressure, wind, and lapse-rate fields that serve as input to the model. The second mode is a *Trajectory* view that executes a six-degree-of-freedom flight simulation with real-time ML-based turbulence correction, mirroring the paired evaluation protocol of Section IV for the three validated speed regimes (Mach 2.8, 4.5, and 8.0).

The demonstration serves three purposes. First, it allows independent verification of PSTNet’s regime-gating behaviour: users can observe how the four expert activations shift as the selected region transitions from equatorial convective conditions to mid-latitude stable stratification to polar regimes,

confirming the physically meaningful routing discussed in Section IV-C. Second, it provides a practical tool for mission planners seeking rapid turbulence assessments at arbitrary waypoints without access to full numerical weather prediction infrastructure. Third, it illustrates the deployment viability of the 552-parameter architecture: the entire model executes with sub-millisecond latency in a standard browser environment, corroborating the embedded-hardware timing results reported in Section IV-G.

## VI. CONCLUSION

This paper introduced PSTNet, a physics-informed mixture-of-experts network for atmospheric turbulence intensity modelling. By coupling a Monin–Obukhov analytical backbone with four lightweight residual experts and a learned gating network, the architecture achieves a mean miss-distance improvement of +2.8% with a 78% win rate across 340 paired 6-DoF simulations, all with only 552 learnable parameters. The effect size (Cohen’s  $d = 0.408$ ,  $p < 10^{-9}$ ) exceeds every baseline, including models with over ten times the capacity. Notably, the gating network recovers classical stability regimes—convective, neutral, stable, and stratospheric—without explicit regime labels, providing transparent and physically grounded explanations suitable for safety-critical applications. The model’s minimal footprint of under 2.5 kB and sub-12  $\mu$ s inference on a Cortex-M7 makes it directly deployable in real-time on-board guidance loops.

All evaluation was conducted in simulation, and flight-test validation is needed to confirm that improvements transfer to real atmospheric conditions. The marginal regression observed in edge-case scenarios suggests that the physics priors may over-constrain predictions in extreme-shear profiles outside the Monin–Obukhov similarity regime. Future work will focus on extending PSTNet to full spectral prediction, incorporating temporal context through recurrent or state-space gating, investigating adaptive expert allocation, and most importantly conducting flight-test validation with instrumented vehicles. Overall, PSTNet demonstrates that embedding domain physics as an architectural prior offers a more efficient and interpretable path to guidance accuracy than scaling model capacity, providing a practical replacement for legacy turbulence look-up tables in next-generation on-board systems.

## REFERENCES

- [1] A. S. Monin and A. M. Obukhov, “Basic laws of turbulent mixing in the surface layer of the atmosphere,” *Trudy Geofizicheskogo Instituta, Akademiya Nauk SSSR*, vol. 24, no. 151, pp. 163–187, 1954.
- [2] T. Foken, “50 years of the Monin–Obukhov similarity theory,” *Boundary-Layer Meteorology*, vol. 119, no. 3, pp. 431–447, 2006. [Online]. Available: <https://doi.org/10.1007/s10546-006-9048-6>
- [3] U.S. Department of Defense, “Military handbook: Flying qualities of piloted aircraft (MIL-HDBK-1797A),” U.S. Department of Defense, Tech. Rep., 1997.

- [Online]. Available: [https://everyspec.com/MIL-HDBK/MIL-HDBK-1700-1799/MIL-HDBK-1797A\\_14349/](https://everyspec.com/MIL-HDBK/MIL-HDBK-1700-1799/MIL-HDBK-1797A_14349/)
- [4] J. H. Friedman, “Greedy function approximation: A gradient boosting machine,” *The Annals of Statistics*, vol. 29, no. 5, pp. 1189–1232, 2001. [Online]. Available: <https://doi.org/10.1214/aos/1013203451>
- [5] A. N. Kolmogorov, “The local structure of turbulence in incompressible viscous fluid for very large Reynolds numbers,” *Doklady Akademii Nauk SSSR*, vol. 30, pp. 301–305, 1941.
- [6] —, “Dissipation of energy in the locally isotropic turbulence,” *Doklady Akademii Nauk SSSR*, vol. 32, pp. 16–18, 1941.
- [7] B. Kriuk and M. Yordanov, “Gelovec: Higher dimensional geometric smoothing for coherent visual feature extraction in image segmentation,” *arXiv preprint arXiv:2505.01057*, 2025.
- [8] N. Shazeer, A. Mirhoseini, K. Maziarz, A. Davis, Q. V. Le, G. E. Hinton, and J. Dean, “Outrageously large neural networks: The sparsely-gated mixture-of-experts layer,” in *5th International Conference on Learning Representations (ICLR 2017)*, 2017. [Online]. Available: <https://openreview.net/forum?id=B1ckMDqIlg>
- [9] E. Perez, F. Strub, H. de Vries, V. Dumoulin, and A. C. Courville, “FiLM: Visual reasoning with a general conditioning layer,” in *Proceedings of the Thirty-Second AAAI Conference on Artificial Intelligence*, 2018. [Online]. Available: <https://doi.org/10.1609/aaai.v32i1.11671>
- [10] NASA Prediction of Worldwide Energy Resources (POWER) Project, “NASA POWER surface meteorology and solar energy reanalysis dataset,” NASA Langley Research Center, 2023. [Online]. Available: <https://power.larc.nasa.gov/>
- [11] S. Pandey, J. Schumacher, and K. R. Sreenivasan, “A perspective on machine learning in turbulent flows,” *Journal of Turbulence*, vol. 21, no. 9-10, pp. 567–584, 2020.
- [12] A. Beck and M. Kurz, “A perspective on machine learning methods in turbulence modeling,” *GAMM-Mitteilungen*, vol. 44, no. 1, p. e202100002, 2021.
- [13] B. D. Tracey, K. Duraisamy, and J. J. Alonso, “A machine learning strategy to assist turbulence model development,” in *53rd AIAA aerospace sciences meeting*, 2015, p. 1287.
- [14] G. P. Ellrod and D. I. Knapp, “An objective clear-air turbulence forecasting technique: Verification and operational use,” *Weather and Forecasting*, vol. 7, no. 1, pp. 150–165, 1992. [Online]. Available: [https://doi.org/10.1175/1520-0434\(1992\)007<0150:AOCATF>2.0.CO;2](https://doi.org/10.1175/1520-0434(1992)007<0150:AOCATF>2.0.CO;2)
- [15] R. Sharman, C. Tebaldi, G. Wiener, and J. Wolff, “An integrated approach to mid- and upper-level turbulence forecasting,” *Weather and Forecasting*, vol. 21, no. 3, pp. 268–287, 2006. [Online]. Available: <https://doi.org/10.1175/WAF924.1>
- [16] P. Spalart, “An old-fashioned framework for machine learning in turbulence modeling,” *arXiv preprint arXiv:2308.00837*, 2023.
- [17] M. Pierzyna, R. Saathof, and S. Basu, “ $\pi$ -ml: a dimensional analysis-based machine learning parameterization of optical turbulence in the atmospheric surface layer,” *Optics Letters*, vol. 48, no. 17, pp. 4484–4487, 2023.
- [18] A. Beck, D. Flad, and C.-D. Munz, “Deep neural networks for data-driven LES closure models,” *Journal of Computational Physics*, vol. 398, p. 108910, 2019. [Online]. Available: <https://doi.org/10.1016/j.jcp.2019.108910>
- [19] J. K. Williams, “Using random forests to diagnose aviation turbulence,” *Machine Learning*, vol. 95, no. 1, pp. 51–70, 2014. [Online]. Available: <https://doi.org/10.1007/s10994-013-5346-7>
- [20] B. Kriuk, “Advancing eurasia fire understanding through machine learning techniques,” *arXiv preprint arXiv:2502.17023*, 2025.
- [21] A. Vaswani, N. Shazeer, N. Parmar, J. Uszkoreit, L. Jones, A. N. Gomez, Ł. Kaiser, and I. Polosukhin, “Attention is all you need,” in *Advances in Neural Information Processing Systems*, vol. 30, 2017. [Online]. Available: <https://arxiv.org/abs/1706.03762>
- [22] B. Kriuk and F. Kriuk, “Deep learning-driven approach for handwritten Chinese character classification,” *arXiv preprint arXiv:2401.17098*, 2024. [Online]. Available: <https://arxiv.org/abs/2401.17098>
- [23] B. Kriuk, “Morphboost: Self-organizing universal gradient boosting with adaptive tree morphing,” *arXiv preprint arXiv:2511.13234*, 2025.
- [24] K. Boris, S. Ketii, and K. Fedor, “Elena: epigenetic learning through evolved neural adaptation,” *Evolutionary Intelligence*, vol. 18, no. 3, p. 50, 2025.
- [25] M. Raissi, P. Perdikaris, and G. E. Karniadakis, “Physics-informed neural networks: A deep learning framework for solving forward and inverse problems involving nonlinear partial differential equations,” *Journal of Computational Physics*, vol. 378, pp. 686–707, 2019. [Online]. Available: <https://doi.org/10.1016/j.jcp.2018.10.045>
- [26] B. Kriuk and F. Kriuk, “Poseidon: Physics-optimized seismic energy inference and detection operating network,” *arXiv preprint arXiv:2601.02264*, 2026.
- [27] P. I. Karpov, C. Huang, I. Sitdikov, C. L. Fryer, S. Woosley, and G. Pilania, “Physics-informed machine learning for modeling turbulence in supernovae,” *The Astrophysical Journal*, vol. 940, no. 1, p. 26, 2022.
- [28] I. Stiperski and M. Calaf, “Generalizing Monin–Obukhov similarity theory for complex atmospheric turbulence,” *Physical Review Letters*, vol. 130, no. 12, p. 124001, 2023. [Online]. Available: <https://doi.org/10.1103/PhysRevLett.130.124001>
- [29] R. B. Stull, *An Introduction to Boundary Layer Meteorology*. Dordrecht: Springer, 1988. [Online]. Available: <https://doi.org/10.1007/978-94-009-3027-8>